
Article:
Adak, Amitava, Singh, Prashant Kumar, Lad, Amit D. et al. (6 more authors) (2016) Efficient transport of femtosecond laser-generated fast electrons in a millimeter thick graphite. Applied Physics Letters. 174101. pp. 1-5. ISSN 0003-6951

https://doi.org/10.1063/1.4966132

Efficient transport of femtosecond laser-generated fast electrons in a millimeter thick graphite

Amitava Adak[1], Prashant Kumar Singh[1], Amit D. Lad[1], Gourab Chatterjee[1], Malay Dalui[1], P. Brijesh,[1] A. P. L. Robinson,[2] John Pasley,[3,2] and G. Ravindra Kumar[1, a)]

[1)] *Tata Institute of Fundamental Research, Dr. Homi Bhabha Road, Colaba, Mumbai-400005, India*

[2)] *Central Laser Facility, Rutherford Appleton Laboratory, Chilton, Didcot, OX10 0QX, United Kingdom*

[3)] *York Plasma Institute, University of York, Heslington, York, YO10 5DQ, United Kingdom*

We demonstrate efficient transport of fast electrons generated by $\sim 10^{18}$ W/cm^2, 30 fs, 800 nm laser pulses through a millimeter thick polycrystalline graphite. Measurements of hot electron spectra at the front side of the graphite target show enhancement in terms of the electron flux and temperature, while the spectra at the rear confirm the ability of the graphite to transport large electron currents over a macroscopic distance of a millimeter. In addition, protons of keV energies are observed at the rear side of such a macroscopically thick target and attributed to the target-normal-sheath-acceleration mechanism.

The advent of chirped pulse amplification[1] has facilitated the exploration of 'extreme' phenomena in intense laser-matter interactions[2] and high-energy-density physics[3]. The transport of the relativistic electrons through a solid material is being investigated to a great extent in various scenarios of intense laser-matter interactions, due to its importance in fast ignition[4] of inertial confinement fusion and other applications like energetic ion-production[5]. However, various instabilities cause strong inhibition in the propagation of the fast electrons, resulting in filamentation[6–8] of the fast electron beam over a length of a few tens of microns[9].

Recently several experiments with innovative target design have been performed for achieving efficient transport of fast electrons[10–13]. Chatterjee *et. al.*[12] used polarimetric measurements of giant magnetic fields at the target rear to show that aligned carbon-nanotube arrays possess the capability to transport mega-ampere electron currents over a distance as large as a millimeter. However, intricate target designs can be challenging to fabricate and are not amenable to mass manufacturing techniques, thereby reiterating the need for simple targets.

In this letter, we demonstrate efficient generation and macroscopic transport of fast electrons in a 1 mm-thick polycrystalline graphite target and compare the results with those from aluminium. Measurements of hot electron spectra at the front side of the graphite target show enhancement in terms of the electron flux and temperature, while the spectra at the rear confirm the ability of the graphite to transport large electron currents over a macroscopic distance of a millimeter. A time-of-flight (TOF) ion measurement at the rear side of the graphite target could be attributed to target-normal-sheath-acceleration (TNSA), which is unusual for such a thick target.

The experiment was carried out with a chirped-pulse-amplification-based 20 terawatt Ti:sapphire laser system at the Tata Institute of Fundamental Research, which can provide intense laser pulses (30 fs, $\lambda = 800$ nm) at a repetition rate of 10 Hz. A 1 mm-thick graphite (and aluminium) target with transverse extent of 4×4 cm^2 was irradiated by p-polarized pump pulse, focused to a 14 μm spot (FWHM) by an $f/3$ off-axis parabolic mirror at an angle of incidence of 45° (Fig. 1 a). A peak intensity of $I_L \sim 1.5 \times 10^{18}$ W/cm^2 was achieved on the target with a nanosecond intensity contrast of 5×10^{-6}.

The experimental setup comprised (a) magnet electron spectrometers (ESMs) and (b) a channel electron multiplier (CEM) for TOF ion measurements. In an independent measurement, an image plate (IP) was placed surrounding the target in a cylindrical geometry (schematic in Fig. 1(b)), spanning an angle of $\sim 150°$, in order to obtain the fast electron angular distribution at the target rear. Each electron spectrum was obtained by averaging 200 laser shots, whereas time-of-flight (TOF) measurements for ions were carried out in single-shot mode by the CEM.

Figure 1(c) shows a schematic of an ESM. Energetic electrons spatially selected by an aperture pass through a region of uniform magnetic field of 0.1 tesla in vacuum. The electron trajectories bend according to their kinetic energy and are incident on an IP-strip (henceforth referred to as ESM-IP), which is read by an IP reader (FLA-7000 of FUJIFILM) to obtain the electron energy spectrum. Each ESM-IP was covered with a 12 μm-thick aluminium foil to reduce the background noise. ESM-1 was placed at the target front in the target normal direction at a distance of 90 cm. ESM-2 and ESM-3 were placed at the rear of the target along the target normal at a distance of 18 cm and along the laser propagation direction at a distance of 20 cm respectively (Fig. 1(a)). The CEM was placed at the rear of the target along near normal direction at a distance of 30 cm.

We present the results of fast electron measurements at the rear of the 1 mm-thick graphite target in Fig. 2. Each raw-trace for the ESM-IP is achieved by accumulating fast electrons for 200 laser shots. The raw-traces for the 1 mm-thick graphite target in ESM-2 and

[a)] Electronic mail: grk@tifr.res.in

ESM-3 are shown in Fig. 2(b) and Fig. 2(c) respectively. For aluminium, hardly any signal was observed over the background noise (Fig. 2(d)). Our earlier measurements with a millimeter-thick amorphous carbon target (in a similar experimental condition) also showed no detectable electron in the rear side[12]. For graphite, on the other hand, the electron spectra inferred from the raw-traces (shown in Fig. 2(a) for both ESM-2 and ESM-3) show clear, strong signals. Each electron spectrum shows two-temperature distribution with characteristic temperatures of – (a) 273 keV and 923 keV along the target rear-normal direction and (b) 158 keV and 1174 keV along the laser propagation direction. The total number of electrons per laser shot per solid angle in ESM-2 is 9.4×10^6 in the energy range (170-1000) keV with a temperature of 273 keV and 1.2×10^6 in the energy range (1-2) MeV with a temperature of 923 keV. The same in ESM-3 is 3.4×10^6 in the energy range (170-570) keV with a temperature of 158 keV and 1.7×10^6 in the energy range (570-2000) keV with a temperature of 1174 keV. In a similar experimental condition, the rear side electron spectrum for a much thinner aluminium target (10 μm-thick) shows a single temperature of only 127 keV (inset of Fig. 2(a)).

The angular distribution of the fast electrons, transported through the 1 mm-thick graphite, was measured (experimental setup in Fig. 1(b)) by an IP, wrapped in a 33 μm-thick aluminium foil. This foil stops the following particles from reaching the IP – (i) electromagnetic radiation up to $\sim$ 1 keV, (ii) electrons upto $\sim$ 65 keV and (iii) protons upto $\sim$ 1.7 MeV. Hence, no laser-generated protons (in the given experimental conditions) could be detected. Assuming the angular distribution of the bremsstrahlung radiation broadly follows that of the hot electrons-trajectory, the signal on the IP-image in Fig. 3(b) can be attributed to a combined measurement of the bremsstrahlung and hot electron distributions. The laser propagation direction (0°) and the rear-normal direction (315°) are indicated in the image by white markers. The vertical line-out of this image is shown in a polar plot (blue curve in Fig. 3(a)), where the radius indicates the flux of electrons in arbitrary units as a function of angle. The angular divergence is measured to be $\alpha_{1/2} = 68°$ (half-angle corresponding to the half-width-at-half-maxima).

Figure 4(a) compares the electron spectra measured by ESM-1 at the front side of 1 mm-thick graphite and 1 mm-thick aluminium. The hot electron spectrum for graphite shows an enhancement both in temperature and in flux for the electron energy-range shown in Fig. 4(a), although of the same order of magnitude, compared to aluminium. Unprocessed ESM-traces (aggregated signal for 200 laser shots) for both the targets are also shown in Fig. 4(a). Therefore the drastic difference at the rear side measurements certainly cannot be because of the difference of front side laser absorption which is further investigated and emphasized by hydro simulations described below.

1D radiation hydrodynamic simulations of the laser prepulse interaction with the target surface show that significant plasma formation will take place prior to the arrival of the main pulse in both graphite and aluminium. Density scale-lengths will be similar for the two materials at the time of arrival of the main pulse. Based upon this we do not think that the differences in transport observed can be explained by consideration of the front surface interaction since we have no reason to suggest that this will be majorly different for the two materials considered here. Differences in the bulk material therefore must be examined to in order to explain the electron transport results.

We have attempted to gain greater insights into the physical mechanism underlying our experimental observations by carrying out a number of numerical simulations. One set of these simulations was focused on the physics in the solid density target that arise due to the propagation of the high current fast electron beam. These simulations were conducted using the 3D particle-based hybrid code, ZEPHYROS. The burst of fast electrons generated by the main laser pulse, being 30 fs in duration is too short to generate magnetic fields, or other effects, that affect its own dynamics (a conclusion that had been reached in separate studies[2,3,12]). The investigation therefore concentrated its efforts on the possibility that hot electron generation preceding the main pulse (but still on a sub-ps timescale) could have produced magnetic fields or target heating that could account for the experimental results. We modelled a pre-pulse of intensity 3×10^{17} W/cm^2 with a duration of 500 fs and also assumed that the temperature of the fast electrons generated by the pre-pulse was 200 keV. We found that magnetic fields generated prior to the main pulse could affect the electron bunch generated by the main pulse. The peak magnetic flux density was 30% less in the Al target than that in the graphite target. However, the difference in the characteristic spatial extent of the magnetic fields was much more significant, and these could differ by a factor of 2 between Al and graphite (with graphite exhibiting the larger region of magnetic fields as shown in Fig. 4(b)). Furthermore, we found that employing a resistivity curve with features similar to that in McKenna *et al.*[14] for the graphite target lead to a noticeable enhancement in this magnetic field structure. Although this investigation did not result in a complete and conclusive explanation of the experimental results, it does suggest that resistive magnetic field generation by hot electrons remains a viable hypothesis.

Thomson parabola spectrometer measurements with thin foils (7.5 μm-thick Al foils) showed that protons are the predominant species accelerated at the target rear in the energy range (1-200) keV under our experimental conditions. As a result, it would not be erroneous to attribute the signal detected in the CEM to protons. We performed a comparative study of the proton emission at the target rear, along the normal direction, from a 200 μm-thick Al foil and a 1.1 mm-thick graphite piece. We

observed no proton emission from the Al foil, while Fig. 5 shows the energy spectrum of the protons generated from the graphite target. Energetic proton emission from the rear of the graphite target conclusively supports its ability to transport electrons over its millimeter thickness.

In summary, we have studied fast electron transport in a millimeter-thick polycrystalline-graphite target. A high flux of relativistic electrons was observed at the target rear. These results are surprising, given the high thickness of the graphite target and can only be explained by the efficient transport provided by graphite. It is highly challenging to pin point the exact reason of such highly efficient macroscopic transport of hot electrons in graphite and to perform particle simulation over such large scale-length in a polycrystalline medium. However, a 3D particle-based hybrid code shows that magnetic fields generated prior to the main pulse could affect the electron bunch generated by the main pulse. These fields are significant in carbon targets though not in metallic targets. Furthermore, we have experimental indications of the efficiency of the graphite target in laser-generated hot electron transport over a macroscopic length which enables the acceleration of protons to keV energies by the well-known TNSA mechanism at the rear side of the thick graphite target.

GRK acknowledges a J. C. Bose Fellowship grant. Authors acknowledge Prof. M. Krishnamurthy, Subhrangsu Sarkar, T. Madhu Trivikram, Indranil Roy, and Dr. Pranab Kumar Das for their help and discussions.

[1]D. Strickland and G. Mourou, Opt. commun. **55,** 447 (1985).
[2]P. Gibbon, *Short Pulse Laser Interactions With Matter* (Imperial College Press, 2005).
[3]R. P. Drake, *High Energy Density Physics* (Springer-Verlag, Berlin, Heidelberg, 2006).
[4]M. Tabak, J. Hammer, M. E. Glinsky, W. L. Kruer, S. C. Wilks, J. Woodworth, E. M. Campbell, M. D. Perry, and R. J. Mason, Phys. Plasmas **1,** 1626 (1994).
[5]M. Passoni, L. Bertagna, and A. Zani, New J. Phys. **12,** 045012 (2010).
[6]Y. Sentoku, K. Mima, Z. M. Sheng, P. Kaw, K. Nishihara, and K. Nishikawa, Phys. Rev. E **65,** 046408 (2002).
[7]M. Honda J. Meyer-ter-Vehn, and A. Pukhov, Phys. Rev. Lett. **85,** 2128 (2000).
[8]L. Gremillet, G. Bonnaud, and F. Amiranoff, Phys. Plasmas **9,** 941 (2002).
[9]A. Pukhov, Phys. Rev. Lett. **86,** 3562 (2001).
[10]P. K. Singh, G. Chatterjee, A. D. Lad, A. Adak, S. Ahmed, M. Khorasaninejad, M. M. Adachi, K. S. Karim, S. S. Saini, A. K. Sood, and G. R. Kumar, Appl. Phys. Lett. **100,** 244104 (2012).
[11]P. K. Singh, I. Chakraborty, G. Chatterjee, A. Adak, A. D. Lad, P. Brijesh, P. Ayyub, and G. R. Kumar, Phys. Rev. STAB **16,** 063401 (2013).
[12]G. Chatterjee, P. Kumar Singh, S. Ahmed, A. P. L. Robinson, A. D. Lad, S. Mondal, V. Narayanan, I. Srivastava, N. Koratkar, J. Pasley, A. K. Sood, and G. R. Kumar, Phys. Rev. Lett. **108,** 235005 (2012).
[13]S. Kar, A. P. L. Robinson, D. C Carroll, O Lundh, K. Markey, P. McKenna, P. Norreys, and M. Zepf, Phys. Rev. Lett. **102,** 055001 (2009).
[14]P. McKenna, A. P. L. Robinson, D. Neely, M. P. Desjarlais, D. C. Carroll, M. N. Quinn, X. H. Yuan, C. M. Brenner, M. Burza, M. Coury, P. Gallegos, R. J. Gray, K. L. Lancaster, Y. T. Li, X. X. Lin, O. Tresca, and C.-G. Wahlstrom, Phys. Rev. Lett. **106,** 185004 (2011).

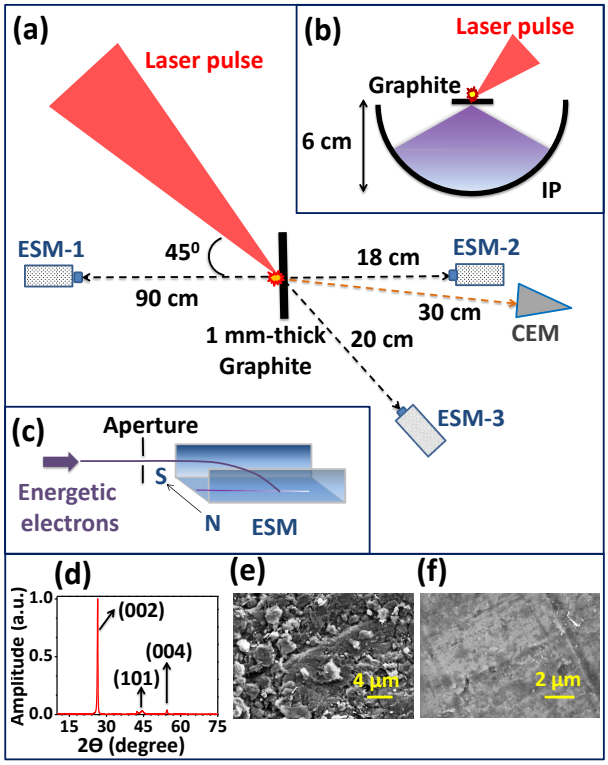

FIG. 1. Experimental setup comprising (a) magnet electron spectrometer (ESM) and channel electron multiplier (CEM) and (b) image plate (IP) covered with 33-μm aluminium foil. (c) Schematic of an ESM. (d) The x-ray diffraction indicates hexagonal structure of the graphite target. The target is polycrystalline in structure. Most of the crystallites (more than 90%) have Bragg planes of type (002), scattering x-rays at an angle of $2\theta = 26.4°$. The corresponding inter-planar spacing is 0.337 nm. The average size of these crystallites is 40 nm. (e) and (f) show the scanning electron microscope (SEM) images of the surface structures of graphite and aluminium respectively.

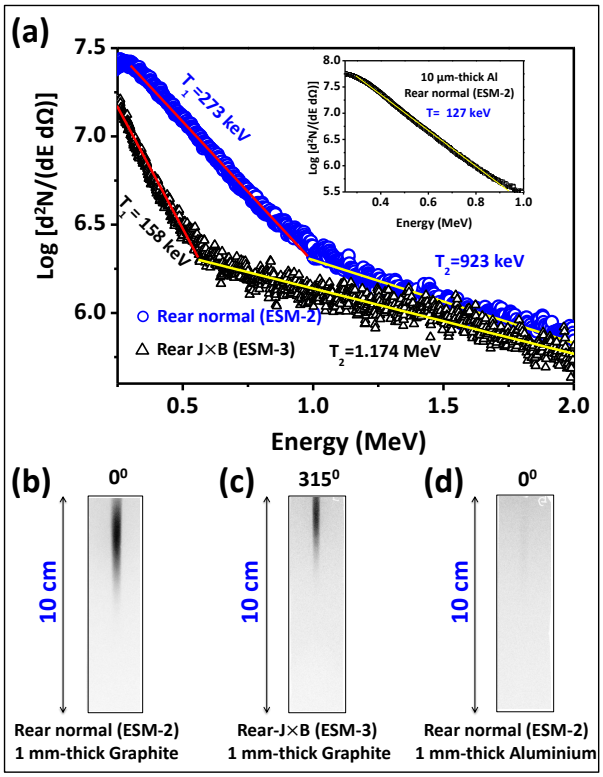

FIG. 2. Electron spectra at the rear side of the graphite target along (a) the target normal direction (blue circles) and (b) the laser propagation or $\boldsymbol{J} \times \boldsymbol{B}$ direction (black triangles). Corresponding raw ESM-traces are shown in (b) and (c). Similar measurements with 1 mm-thick aluminium target could not detect any signal above the threshold level, as shown in (d). Inset in (a) shows the rear side electron spectrum for a 10 μm-thick aluminium

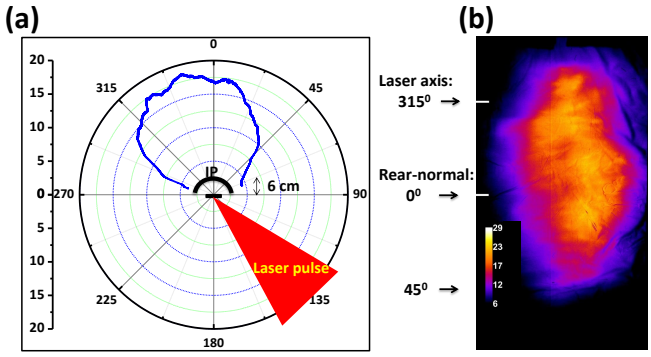

FIG. 3. (a) Polar plot for the angular distribution of the hot electrons emitted from the rear side of the graphite target, calculated by taking the vertical line-out from the IP-image in (b). The color bar in the IP image indicates the flux in arbitrary units.

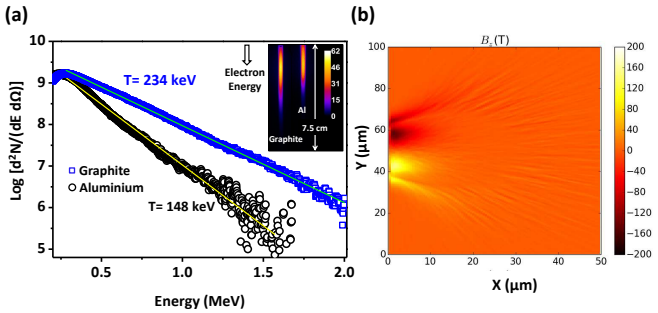

FIG. 4. (a) Electron spectra measured by ESM-1 placed 90 cm away from the target at the target front along the normal direction for graphite (blue squares) and aluminium (black circles). Inset shows the raw ESM traces, where the increasing electron energy is downwards and the color bar indicates the electron flux in arbitrary units. (b) Simulated magnetic fields close to the front surface of graphite target.

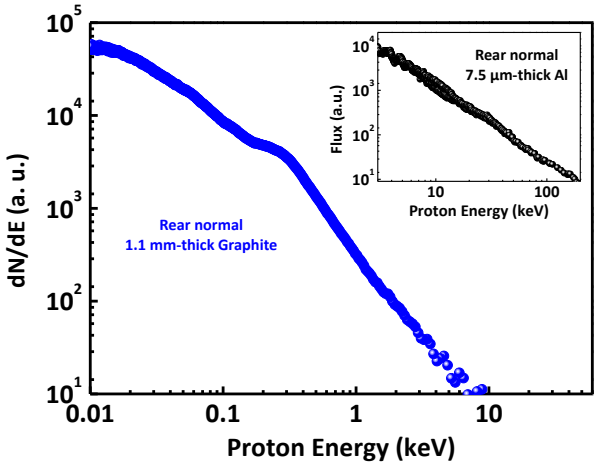

FIG. 5. Energy spectra of the protons accelerated to keV energies at the rear side of 1 mm-thick graphite target. Inset shows the proton spectrum at the rear side of 7.5 μm-thick aluminium foil.